JOURNAL OF GEOPHYSICAL RESEARCH, VOL. 106, NO. C5, PAGES 9385–9391, MAY 15, 2001

Microscale wave breaking and air–water gas transfer

C. J. Zappa, [1,2] W. E. Asher, and A.T. Jessup[1]

Applied Physics Laboratory, University of Washington, Seattle, Washington

Abstract. Laboratory results showing that the air–water gas transfer velocity k is correlated with mean square wave slope have been cited as evidence that a wave-related mechanism regulates k at low to moderate wind speeds [*Jähne et al.*, 1987; *Bock et al.*, 1999]. *Csanady* [1990] has modeled the effect of microscale wave breaking on air–water gas transfer with the result that k is proportional to the fractional surface area covered by surface renewal generated during the breaking process. In this report we investigate the role of microscale wave breaking in gas transfer by determining the correlation between k and A_B, the fractional area coverage of microscale breaking waves. Simultaneous, colocated infrared (IR) and wave slope imagery is used to verify that A_B detected using IR techniques corresponds to the fraction of surface area covered by surface renewal in the wakes of microscale breaking waves. Using measurements of k and A_B made at the University of Washington wind-wave tank at wind speeds from 4.6 to 10.7 m s^{-1}, we show that k is linearly correlated with A_B, regardless of the presence of surfactants. This result is consistent with *Csanady*'s [1990] model and implies that microscale wave breaking is likely a fundamental physical mechanism contributing to gas transfer.

1. Introduction

Air–sea gas exchange plays a crucial role in geochemical cycling, and a robust parameterization of the gas transfer velocity is needed to improve models of global fluxes [*Sarmiento et al.*, 1992; *Kattenberg et al.*, 1996]. The gas flux across an air–water interface is typically expressed as the product of the gas transfer velocity k and the difference between the gas concentration in the air and in the water. The magnitude of k for slightly soluble gases is determined by diffusion through a thin, spatially and temporally varying aqueous concentration boundary layer (CBL), whose thickness is a function of near-surface turbulence and molecular diffusivity. Because energy input from the wind is the primary force that drives air–sea exchange, k is often parameterized in terms of wind speed or wind stress. However, the dependence of k on these wind parameters has been shown to be a function of the concentration of surfactants [*Frew*, 1997], which are ubiquitous.

Microscale wave breaking, or microbreaking [*Banner and Phillips*, 1974], defined as the breaking of steep, wind-forced waves without air entrainment, begins at wind speeds well below the level at which whitecaps appear [*Melville*, 1996]. Laboratory and field observations show microbreaking waves are O(0.1–1 m) in length and O(0.01–0.1 m) in amplitude and have a bore-like crest with parasitic capillary waves riding along the forward face. Based on laboratory measurements showing that k is correlated with the mean square wave slope, *Jähne et al.* [1987] suggested that microbreaking may significantly contribute to k at low to moderate wind speeds. For these wind conditions, k has been theorized to be controlled by enhanced renewal of the CBL in the turbulent wakes of microbreaking waves [*Csanady*, 1990]. *Csanady* [1990] modeled the effect of microscale wave breaking on gas transfer as

$$k = \phi \beta u_* Sc^{-1/2}, \tag{1}$$

where ϕ is the fractional surface area covered by intense wave-induced surface divergence generated during the breaking process, β is a dimensionless constant, u_* is the aqueous friction velocity, and $Sc = \nu/D$ is the Schmidt number, the ratio of the kinematic viscosity of water to the gas diffusivity in water.

Infrared (IR) imaging techniques have been used to study wave breaking over a wide range of scales, from whitecaps to microbreaking [*Jessup et al.*, 1997a; *Jessup et al.*, 1997b]. Here we use simultaneous IR and wave slope imagery to verify that IR techniques can detect and quantify surface renewal due to microbreaking. A thresholding technique, based on the work of *Jessup et al.* [1997b] and described in the following section, is applied to the IR images to estimate the fraction of

[1]Also at the Department of Civil Engineering, University of Washington, Seattle, Washington.

[2]Now at Bigelow Laboratory, Woods Hole Oceanographic Institution, Woods Hole, Massachusetts.

Paper number 2000JC000262.
0148-0227/01/2000JC000262$09.00

surface area A_B in which the aqueous thermal boundary layer, or "skin" layer, is renewed in the wakes of microbreaking waves. While the mean thermal boundary layer thickness is $O(100\ \mu\text{m})$, the optical depth of the detected IR radiation, roughly 20 μm, is of the order of the mean thickness of the CBL. Therefore A_B serves as an indicator of surface renewal that affects the CBL. Assuming that A_B is equivalent to the surface density of breaking-induced divergences ϕ, then a test of (1) is to determine if k scales with A_B.

Furthermore, if the transfer velocity within the wakes of microbreaking waves is significantly greater than that outside the wakes, k should be dependent on the fraction of the water surface covered by the wakes, which we have defined as A_B. A simple partitioning of the contribution to k from the areas inside and outside of the wakes is

$$k = A_B k_B + (1 - A_B)k_0, \tag{2}$$

where k_B is the transfer velocity within A_B and k_0 is the transfer velocity outside of A_B. The surface renewal rate is central to determining k_B and k_0 and is expected to be variable, depending on the intensity of microbreaking and background turbulence. Determining the validity of (2) requires direct measurement of k_B and k_0, which is beyond the scope of this study. However, if (2) is valid and $k_B >> k_0$, then k will be correlated with A_B, and we can conclude that microbreaking contributes significantly to the gas transfer velocity. *Csanady*'s [1990] result in (1) provides a point of reference for the model described in (2) and serves as a basis for scaling k using A_B.

2. Simultaneous IR and Wave Slope Imagery

The ability to detect and quantify extended areas of surface renewal using passive IR imagery depends on the existence of a measurable temperature difference between the bulk water and the water surface, or skin. This bulk–skin temperature difference ΔT is a function of the net heat flux and the wind stress. When the net heat flux is from the water to the air, a cool skin layer is present, and a disruption that mixes water from below results in a warm surface signature. The most intense disruptions will produce the warmest signatures, with complete disruption resulting in a maximum temperature equal to the bulk temperature [*Zappa et al.*, 1998]. In the laboratory we controlled the magnitude and sign of ΔT by heating the water so that it was roughly 10°C warmer than the air, which typically results in a ΔT of 1°–2°C.

The correspondence of the wake of a microscale breaking wave with its infrared signature is demonstrated by the example of simultaneous infrared and wave slope imagery in Figure 1. The measurements were made in the Air-Sea Interaction Research Facility at the NASA Goddard Space Flight Center, Wallops Flight Facility, at 5.6 m fetch for a wind speed of 5.5 m s^{-1}. The IR imagery was acquired using an Amber Radiance HS imager with a focal plane array that operates at wave-

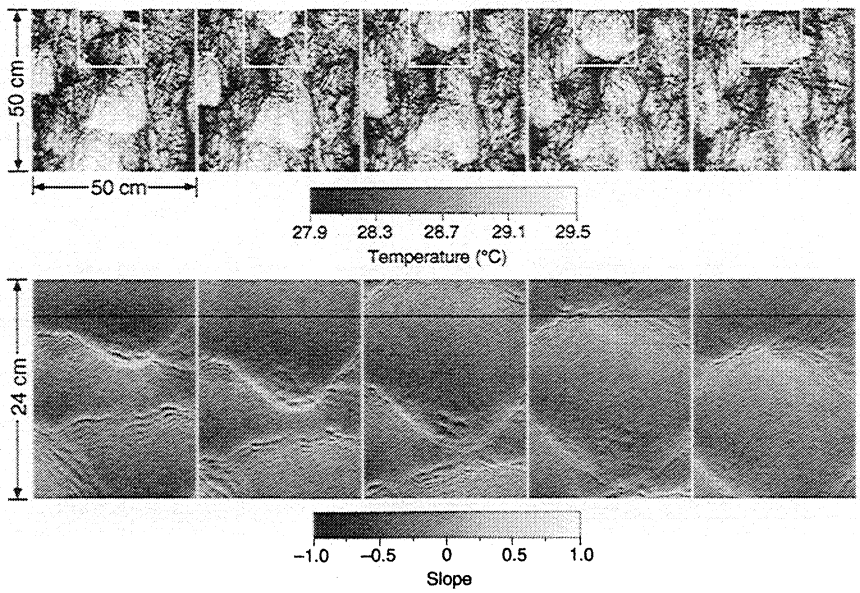

Figure 1. (top) Sequences of simultaneous infrared and (bottom) wave slope imagery for $U = 5.5$ m s^{-1}, measured at a fetch of 5.6 m along the centerline of the tank and at a height above the cleaned water surface of 30 cm. Wind direction is from top to bottom. The white box in the IR images is the overlapping region of the slope measurements and corresponds to the area below the black line in the slope images. Other parameters are bulk–skin temperature difference $\Delta T = 0.6$°C; air–water temperature difference, $\Delta T_{aw} = -5.9$°C; water temperature $T_w = 27.9$°C; relative humidity RH = 47.3%; peak wave frequency $f_p = 3.58$ Hz; and root-mean-square surface displacement RMS $\eta = 0.4$ cm.

lengths of 3–5 μm and has a noise level of 0.025°C. The surface temperature was derived from the measured radiance and is proportional to image intensity. The white box at the top of the IR images corresponds to the area of the slope imagery. The slope measurements were made using an optical imaging technique developed by *Keller and Gotwols* [1983] and modernized by *Jähne and Riemer* [1990] in which the surface slope in the along-wind direction is proportional to the image intensity.

The water surface was dominated by wind-generated gravity waves with lengths of $O(0.1$ m) that were accompanied by parasitic capillary waves. Parasitic capillary waves are generated by short gravity waves and have been modeled as a perturbation, arising from local surface tension forces on a steep gravity wave, that produces a train of capillary waves ahead of the gravity wave crest [*Longuet-Higgins*, 1963]. Parasitic capillary waves are, by definition, not generated by wind forcing, though they may be augmented in wind-forced conditions. In the slope images the forward face of the crest of an individual gravity wave appears as a relatively broad, bright band propagating downwind. Capillary waves appear as fine bands of alternating light and dark lines. The IR images show warm, distinct patches superimposed on a background of less-distinct cool patches and warm fine-scale structures. The surface temperature within the warm patches is consistently greater than that of the background features. Therefore the warm patches can be readily detected by thresholding the IR images at a level that is greater than the mean temperature of the image.

Observations have indicated that when the aqueous thermal boundary layer at the air-water interface is disturbed by a turbulent event, the skin temperature T_s measured by a radiometric device is approximately equal to the bulk water temperature T_w [see *Zappa et al.*, 1998]. The knowledge of T_s previous to and following the disruption allows one to estimate the bulk–skin temperature difference $\Delta T = T_w - T_s$. Therefore, since microscale wave breaking is a turbulent event that causes the disruption of the thermal boundary layer, a threshold based upon ΔT is an appropriate choice. Furthermore, according to surface renewal theory, water at the surface is continually and randomly renewed with water from the bulk. Thus the surface is continually being disrupted on a scale comparable to the eddy size, and the variation in the temperature with an infrared image should also give an estimate of ΔT.

The threshold temperature T_{thresh} for a given data set can be defined as $T_{\text{thresh}} = T_{\text{base}} + jT_{\text{offset}}$, where T_{base} can be defined either as the mean temperature in an image T_{mean} or as a measure of the minimum temperature in an image T_{min} [*Zappa*, 1999]. T_{offset} is based on a measure of ΔT, and j is a parameter chosen such that $0 < jT_{\text{offset}} < \Delta T$. For the images shown in Figure 1, T_{base} is taken as T_{min}, defined as the mean of the lowest 1% of the image temperature distribution, to represent the surface temperature closest to the undisturbed state. T_{offset} is calculated as the standard deviation of the temperature distribution in the image. Using these values for T_{offset} and T_{base}, for all wind speeds (U ranged from 4.2 to 9.3 m s^{-1}) and all surface conditions during the Wallops Flight Facility experiments, a value of $j = 3.5$ reliably identified the warmest areas of the images thought to be the wakes of microscale breaking waves.

The warm patches appear and evolve in conjunction with the crests of individual wind waves, although not all wave crests produce warm patches. In Figure 2 the IR images have been enlarged to show only the region that overlaps the slope images. A contour obtained by thresholding the IR images at a level T_{thresh} defined above is superimposed on both sequences. This contour level outlines a distinct warm area that is growing in

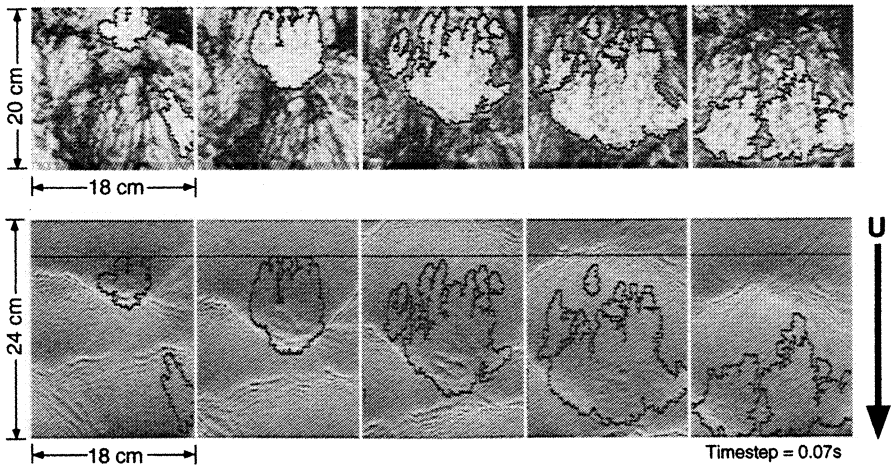

Figure 2. Same as Figure 1 except that the IR images have been enlarged to show only the overlap region. Overlaid in both sequences is a temperature contour outlining water warmer than the mean level, which corresponds to a portion of the turbulent wake of a microbreaking wave. The leading edge of the outlined region coincides with the steep crest of the microbreaking wave.

size and propagating downwind. The leading edge of the patch propagates with the steep forward face of the wave crest in the slope image. The trailing edge of the patch also propagates downwind but at a slower speed than the leading edge. If the threshold is lowered by choosing a smaller value for j, a larger area behind the crest is detected. If the threshold is raised by choosing a larger value for j, a smaller area behind the crest is detected, but the region at the forward face persists, since the leading edge is the warmest part of the patch.

The warm patches associated with individual waves are distinct, intense regions of surface renewal that are left behind by steep wind-generated waves. After the patches are generated, they decay into the background. Our observations imply that the distinct regions of warm water detected in the IR imagery that occur behind steep wind-wave crests are the turbulent wakes of microbreaking waves. If this true, then we can obtain a measure of the surface area affected by microbreaking A_B by applying a threshold to the IR images that outlines the large regions of warmest temperature. In order to minimize the contribution to A_B from small-scale features not associated with microbreaking, the IR images are spatially filtered such that surface renewal events smaller than $O(0.01$ m) are not detected. Then A_B is the ratio of the area of the outlined regions to the total area of the image. For a useful range of thresholds we verified that the overwhelming majority of the detected area is due to the large, distinct patches of enhanced surface renewal that occur in conjunction with steep waves.

3. Measurements of Microbreaking Coverage and Gas Transfer Velocity

A detailed analysis of the measurements at Wallops Flight Facility is the subject of a forthcoming report. For the analysis in this paper we use measurements of A_B and k made in the wind-wave tank at the University of Washington Harris Hydraulics Laboratory. The tank is 9.1 m long, 1.2 m wide, and 0.9 m deep and is equipped with a wind flume, a wave-absorbing beach, and a water heater. The IR imagery was recorded using the previously mentioned imager. The facility is instrumented to measure the parameters listed in Table 1, which summarizes the conditions during the 13 experiments in this study. Before each experiment the filtered tapwater in the tank was heated, and the surface was vacuumed to remove accumulated surface contaminants. Biological activity was minimized in all but two experiments by sterilizing the water with approximately 0.5 kg of sodium hypochlorite. As a further precaution against inadvertent surface contamination, the tank was drained, cleaned, and refilled on a weekly basis. For the controlled surfactant-influenced experiments, 1 g m^{-3} of Triton X-100 was added.

During the measurements at Harris, ΔT was measured directly using bulk thermistors and calibrated IR radiometers. Therefore T_{thresh} was calculated using T_{base} equal to the mean temperature of each image, T_{offset} equal to the measured ΔT, and $j = 0.1$. Although wave slope measurements were not available in this facility, a comprehensive survey of the thresholded IR images showed that the area detected by the chosen threshold was consistently dominated by renewal due to microbreaking. Similar to the observations described in Figures 1 and 2 from the Wallops Flight Facility, the leading edge of the disturbed region in the IR images propagated at the phase speed of the dominant wave, and the scale of the patch was comparable to the dominant wavelength.

Figure 3 shows A_B versus the wind speed U. For the cleaned surfaces (open markers), A_B increases from 0.10 to 0.25 as U increased from 4.6 to 10.7 m s^{-1}. For the controlled surfactant-influenced surfaces (solid markers), A_B is significantly lower at a given U, consistent with the known ability of surfactants to damp gravity-capillary waves [*Alpers and Hühnerfuss,* 1989]. The two experiments conducted using unsterilized water (shaded markers) also result in decreased A_B, suggesting the presence of surface-active material produced by biological activity.

Bulk gas transfer velocities were determined for He and SF_6 by supersaturating the water with the gases and measuring the decrease in their concentration over time [*Asher et al.,* 1996]. Concentration measurements were made as a function of fetch and depth to verify that the tank was well mixed and homogeneous. Samples were drawn at three evenly spaced depths at the test section, which was located at 5 m fetch, and at

Table 1. Average Conditions During Each Experiment[a]

U, m s^{-1}	ΔT, °C	ΔT_{aw}, °C	T_w, °C	RH, %	f_p, Hz	RMS η, cm
4.6	1.8	−12.0	30.2	59.1	5.0	0.11
4.6	2.1	−12.7	30.2	47.4	4.8	0.13
6.3	1.6	−11.0	30.1	61.9	3.9	0.23
6.6	1.8	−12.3	30.3	40.6	3.8	0.18
6.8	2.0	−12.2	29.5	43.3	3.7	0.27
8.7	1.7	−12.4	30.4	43.0	3.3	0.31
8.7	1.6	−9.2	29.8	34.3	3.4	0.30
10.5	1.4	−11.9	30.0	47.5	2.9	0.58
10.5	1.7	−10.5	30.5	40.6	2.9	0.30
10.6	1.4	−7.9	29.4	43.5	3.0	0.37
10.6	1.7	−10.0	29.4	37.4	2.9	0.54
10.6	1.4	−7.1	28.7	29.9	3.0	0.30
10.7	1.0	−6.9	28.5	36.1	2.9	0.58

[a] Conditions are listed by wind speed U measured along the centerline of the tank at 4.67 m fetch and a height above the water surface of 30 cm. Other parameters are bulk–skin temperature difference ΔT, air–water temperature difference ΔT_{aw}, water temperature T_w, relative humidity RH, peak wave frequency f_p, and root-mean-square surface displacement, RMS η.

mid-depth both 4 m upstream and 3.5 m downstream of the test section. At each sampling time t a tank-averaged concentration $C(t)$ was calculated from the individual concentrations at the five sampling locations. The tank-averaged k was calculated as the slope of the line $-h\ln[C(t)/C(0)]$ versus t, where $C(0)$ is the initial concentration in the water and h is the tank depth. Figure 4 shows k versus U for He and SF_6. Consistent with previous results [*Frew*, 1997], k is lower for a given U in the surfactant-influenced experiments than in the cleaned surface ones. Figure 4 demonstrates the difficulty of using wind speed to parameterize gas exchange since k is a multivalued function of U.

Figure 5 shows k versus A_B for He (circles) and SF_6 (triangles). In contrast to the multivalued behavior of k with respect to U seen in Figure 4, in Figure 5 k is a single-valued function of A_B for each gas. Within experimental error, the correlation is independent of surface cleanliness, with a linear coefficient of determination between k and A_B of 0.98 for He and 0.97 for SF_6. Furthermore, the slope of the linear relationship between k and A_B does not change as the threshold for determining A_B is varied.

4. Discussion

The optical depth of the IR radiation measured by the imager is 20 μm. Therefore skin layer disruptions that produce a warm signature in the IR imagery are regions where the fluid is renewed within 20 μm of the surface, which is of the same order as the CBL thickness. Because the wakes of microbreaking waves are the warmest features in the IR imagery, the renewal in the wakes is more intense than the renewal due to the small-scale features in the background. Our results show that 10–25% of the surface is affected by microbreaking and that the fractional area of coverage correlates with the gas transfer velocity. Since the simultaneous IR and slope imagery shows that A_B provides a measure of the water surface area affected by microbreaking, the correlation between k and A_B implies that microbreaking contributes to the increase in k with U. The results warrant further investigation of the microbreaking process including the effect of the distribution of intensity and frequency of occurrence of microbreaking on k. Quantifying the fractional contribution of microbreaking to gas

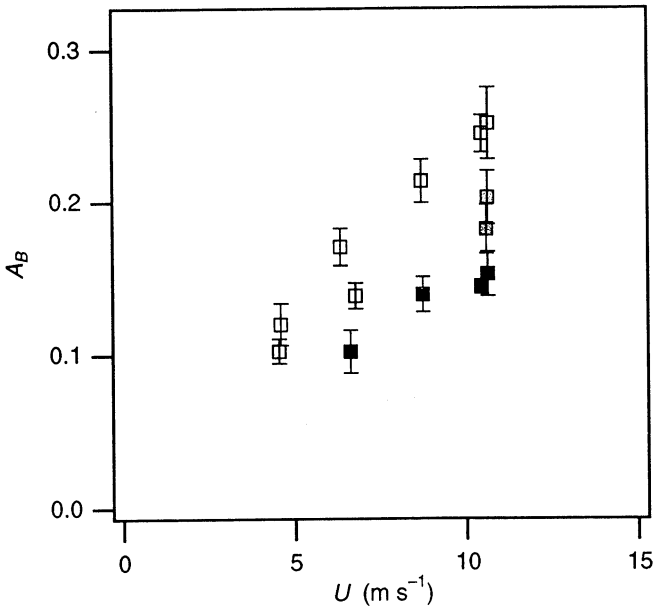

Figure 3. Fraction of surface area covered by microbreaking A_B versus wind speed U. Open markers are for a cleaned surface, shaded markers are for a surface affected by biological activity, and solid markers are for a surface influenced by surfactants. Each point is the mean for one experiment, and the error bars are the standard deviation of the means.

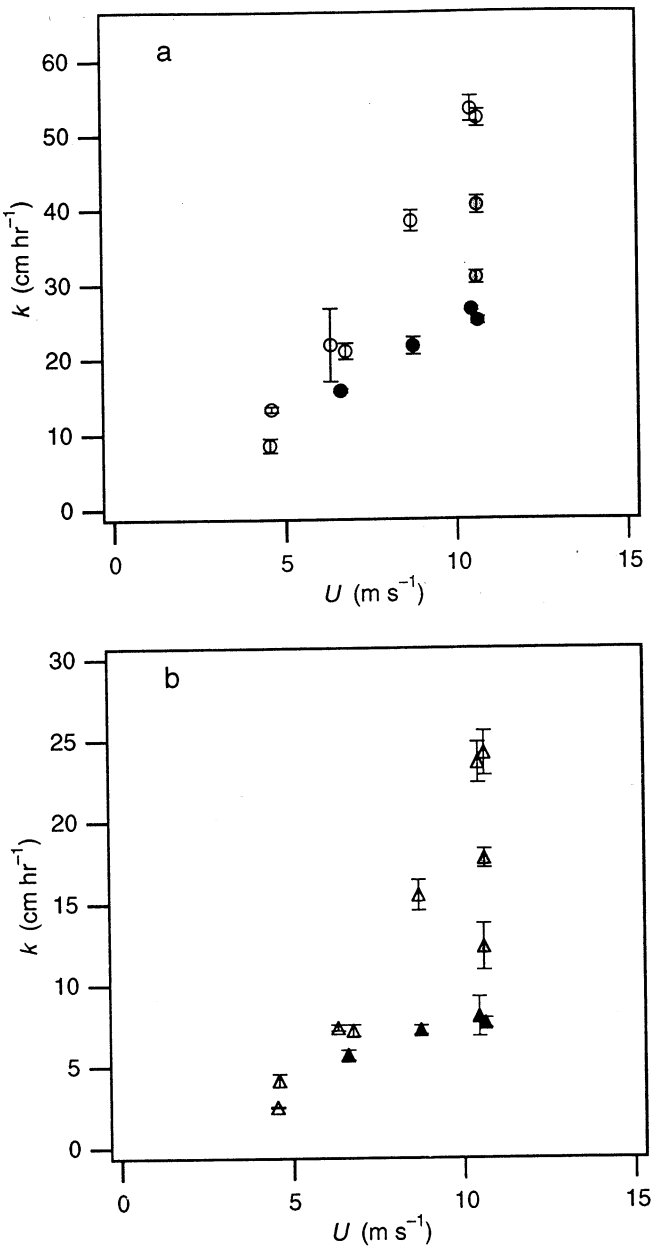

Figure 4. Bulk gas transfer velocity k versus wind speed U for (a) He and (b) SF_6. Symbol shading is as in Figure 3. The error bars show the standard error of the fit from the linear regression $-h\ln[C(t)/C(0)]$ versus time t.

exchange must await direct measurement of k_B and k_0 and their respective surface renewal rates. Nonetheless, our results are the first experimental evidence showing a dependence of the gas transfer velocity on a quantitative measure of microscale wave breaking and are consistent with the model proposed by *Csanady* [1990], namely, that k scales with A_B.

The example of simultaneous IR and slope imagery in Figures 1 and 2 suggests that significant increases in local wave slope are associated with microbreaking waves. If the contribution of microbreaking waves to the mean square wave slope is significantly greater than that from waves that are not breaking, then the correlation between k and A_B shown in Figure 5 may explain why wave slope has been observed to correlate with k.

Models and experiments have shown that the dependence of k on diffusivity can be expressed as Sc^{-n}, where Sc is the Schmidt number of the gas. Conceptual models show that the exponent n ranges from $^1/_2$ to $^2/_3$, depending primarily on surface cleanliness. (For a clean surface that approximates the free surface boundary condition, $n = {}^1/_2$. For a surfactant-influenced surface that approximates the rigid boundary condition, $n = {}^2/_3$ [*Jähne and Haußecker,* 1998].) From Figure 5 alone therefore it is unclear whether n is a single-valued function of A_B because the cleaned and surfactant-influenced points are interspersed. Because He and SF_6 have different Sc values, n can be calculated from their measured k values and their known Sc. For a particular A_B value in Figure 5, $n = \ln[k(SF_6)/k(He)]/\ln[Sc(He)/Sc(SF_6)]$. Figure 6 shows n calculated in this manner plotted versus A_B. The data show that n is indeed a single-valued function of A_B and that it decreases from roughly $^2/_3$ to $^1/_2$ as A_B increases.

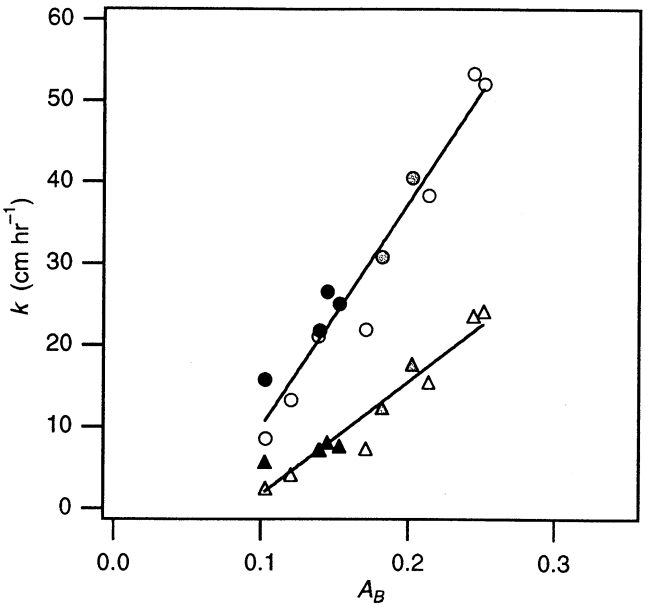

Figure 5. Gas transfer velocity k versus fractional area coverage A_B for He (circles) and SF_6 (triangles). Symbol shading is as in Figure 3. The lines show the linear fit for each gas.

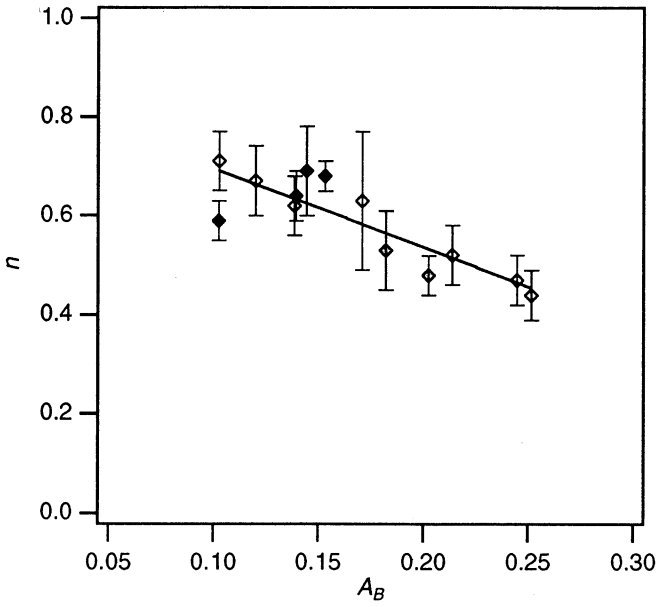

Figure 6. The Schmidt number exponent n versus fractional area coverage A_B. The linear regression shown is $n = 0.855 - 1.591A_B$ with a linear coefficient of determination of 0.86. Symbol shading is as in Figure 3.

5. Conclusion

We have found that the fraction of the surface area covered by microbreaking is linearly correlated with the gas transfer velocity. Furthermore, the correlation is unaffected by the presence of surfactants. This result is the first quantitative evidence that microbreaking is an important wave-related mechanism that influences the gas transfer velocity at low to moderate wind speeds. Using the IR signature of microbreaking to investigate the mechanism by which it contributes to gas transfer offers advantages over using wave statistics, such as slope, because the IR signature is a direct result of the renewal process that affects the gas flux. The widespread occurrence of microbreaking in nature suggests that its cumulative effect on air–sea gas exchange may be significant. However, the laboratory wave conditions for the wind speed range studied in these experiments may not be directly comparable to field conditions at similar wind speeds. Field measurements employing this remote-sensing technique should be made to determine the extent to which our results are applicable in the field.

Acknowledgments. The authors wish to thank S. Long of NASA GSFC-WFF for use of the Air-Sea Interaction Research Facility and J. Klinke of Scripps Institution of Oceanography for providing the wave slope imagery. This work was supported by the National Science Foundation, the Office of Naval Research, the National Aeronautics and Space Administration, and the Applied Physics Laboratory at the University of Washington.

References

Alpers, W., and H. Hühnerfuss, The damping of ocean waves by surface films: A new look at an old problem, *J. Geophys. Res., 94,* 6251–6265, 1989.

Asher, W. E., L. M. Karle, B. J. Higgins, P. J. Farley, E. C. Monahan, and I. S. Leifer, The influence of bubble plumes on air-seawater gas transfer velocities, *J. Geophys. Res., 101,* 12,027–12,041, 1996.

Banner, M. L., and O. M. Phillips, On the incipient breaking of small scale waves, *J. Fluid Mech., 65,* 647–656, 1974.

Bock, E. J., T. Hara, N. M. Frew, and W. R. McGillis, Relationship between air–sea gas transfer and short wind waves, *J. Geophys. Res., 104,* 25821–25831, 1999.

Csanady, G. T., The role of breaking wavelets in air–sea gas transfer, *J. Geophys. Res., 95,* 749–759, 1990.

Frew, N. M., The role of organic films in air-sea exchange, in *The Sea Surface and Global Change,* edited by P. S. Liss and R. A. Duce, pp. 121–172, Cambridge Univ. Press, New York, 1997.

Jähne, B., and H. Haußecker, Air–water gas exchange, *Annu. Rev. Fluid Mech., 30,* 443–468, 1998.

Jähne, B., and K. Riemer, Two-dimensional wave number spectra of small-scale water surface waves, *J. Geophys. Res., 95,* 11,531–11,546, 1990.

Jähne, B., K. O. Munnich, R. Bosinger, A. Dutzi, W. Huber, and P. Libner, On the parameters influencing air–water gas exchange, *J. Geophys. Res., 92,* 1937–1949, 1987.

Jessup, A. T., C. J. Zappa, M. R. Loewen, and V. Hesany, Infrared remote sensing of breaking waves, *Nature, 385,* 52–55, 1997a.

Jessup, A. T., C. J. Zappa, and H. Yeh, Defining and quantifying microscale wave breaking with infrared imagery, *J. Geophys. Res., 102,* 23,145–23,154, 1997b.

Kattenberg, A., F. Giorgi, H. Grassl, G. A. Meehl, J. F. B. Mitchell, R. J. Stouffer, T. Tokioka, A. J. Weaver, and T. M. L. Wigley, Climate models—projections of future climate, in *Climate Change 1995: The Science of Climate Change,* edited by J. T. Houghton et al., pp. 285–357, Cambridge Univ. Press, New York, 1996.

Keller, W. C., and B. L. Gotwols, Two-dimensional optical measurement of wave slope, *Appl. Opt., 22,* 3476–3478, 1983.

Longuet-Higgins, M. S., The generation of capillary waves by steep gravity waves, *J. Fluid Mech., 16,* 138–159, 1963.

Melville, W. K., The role of surface-wave breaking in air–sea interaction, *Annu. Rev. Fluid Mech., 28,* 279–321, 1996.

Sarmiento, J. L., J. C. Orr, and U. Siegenthaler, A perturbation simulation of CO_2 uptake in an ocean general circulation model, *J. Geophys. Res., 97,* 3621–3645, 1992.

Zappa, C. J., Microscale wave breaking and its effect on air-water gas transfer using infrared imagery, Ph.D. thesis, Univ. of Wash., Seattle, 1999.

Zappa, C. J., A. T. Jessup, and H. H. Yeh, Skin-layer recovery of free-surface wakes: Relationship to surface renewal and dependence on heat flux and background turbulence, *J. Geophys. Res., 103,* 21,711–21,722, 1998.

W. E. Asher, Applied Physics Laboratory, University of Washington, 1013 N.E. 40th Street, Seattle, WA 98105-6698. (e-mail: asher@apl.washington.edu)

A. T. Jessup, Applied Physics Laboratory and Department of Civil Engineering, University of Washington, 1013 N.E. 40th Street, Seattle, WA 98105-6698. (e-mail: jessup@apl.washington.edu)

C. J. Zappa, Woods Hole Oceanographic Institution, Bigelow Laboratory, MS 9, Woods Hole, MA 02543 (e-mail: czappa@whoi.edu)

(Received January 26, 2000; revised December 19, 2000; accepted January 16, 2001.)